Accepted Manuscript

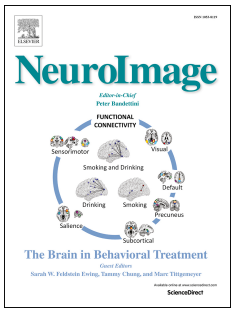

Introducing axonal myelination in connectomics: A preliminary analysis of g-ratio distribution in healthy subjects

Matteo Mancini, Giovanni Giulietti, Nicholas Dowell, Barbara Spanò, Neil Harrison, Marco Bozzali, Mara Cercignani

PII: S1053-8119(17)30766-8

DOI: 10.1016/j.neuroimage.2017.09.018

Reference: YNIMG 14331

To appear in: *NeuroImage*

Received Date: 2 June 2017

Accepted Date: 8 September 2017

Please cite this article as: Mancini, M., Giulietti, G., Dowell, N., Spanò, B., Harrison, N., Bozzali, M., Cercignani, M., Introducing axonal myelination in connectomics: A preliminary analysis of g-ratio distribution in healthy subjects, *NeuroImage* (2017), doi: 10.1016/j.neuroimage.2017.09.018.

This is a PDF file of an unedited manuscript that has been accepted for publication. As a service to our customers we are providing this early version of the manuscript. The manuscript will undergo copyediting, typesetting, and review of the resulting proof before it is published in its final form. Please note that during the production process errors may be discovered which could affect the content, and all legal disclaimers that apply to the journal pertain.

ACCEPTED MANUSCRIPT

Introducing axonal myelination in connectomics: a preliminary analysis of g-ratio distribution in healthy subjects

Matteo Mancini[1,2], *Giovanni Giulietti*[1], *Nicholas Dowell*[2], *Barbara Spanò*[1], *Neil Harrison*[2], *Marco Bozzali*[1,2], *and Mara Cercignani*[1,2]

[1]*Neuroimaging Laboratory, Santa Lucia Foundation, Rome, Italy*

[2]*Department of Neuroscience, Brighton and Sussex Medical School, University of Sussex, Brighton, UK*

***Corresponding author:**

Matteo Mancini

Neuroimaging Laboratory, IRCCS Santa Lucia Foundation

Via Ardeatina, 306, 00179 Rome, Italy

Telephone number: +39 06 5150 1324; Fax number: +39 06 5150 1213

E-mail: matteo.mancini@uniroma3.it

Acknowledgements: This work was funded by a grant from the Italian Ministry of Health (RF-2013-02358409) awarded to Mara Cercignani.

ACCEPTED MANUSCRIPT

Abstract

Microstructural imaging and connectomics are two research areas that hold great potential for investigating brain structure and function. Combining these two approaches can lead to a better and more complete characterization of the brain as a network. The aim of this work is characterizing the connectome from a novel perspective using the myelination measure given by the g-ratio. The g-ratio is the ratio of the inner to the outer diameters of a myelinated axon, whose aggregated value can now be estimated in vivo using MRI. In two different datasets of healthy subjects, we reconstructed the structural connectome and then used the g-ratio estimated from diffusion and magnetization transfer data to characterise the network structure. Significant characteristics of g-ratio weighted graphs emerged. First, the g-ratio distribution across the edges of the graph did not show the power-law distribution observed using the number of streamlines as a weight. Second, connections involving regions related to motor and sensory functions were the highest in myelin content. We also observed significant differences in terms of the hub structure and the rich-club organization suggesting that connections involving hub regions present higher myelination than peripheral connections. Taken together, these findings offer a characterization of g-ratio distribution across the connectome in healthy subjects and lay the foundations for further investigating plasticity and pathology using a similar approach.

Keywords: g-ratio; connectome; myelin; graph theory; microstructure; structural connectivity; diffusion weighted imaging.

Abbreviations: DWI: diffusion weighted imaging; NODDI: neurite orientation dispersion and density imaging; qMT: quantitative magnetization transfer; NOS: number of streamlines.

1. Introduction

The characterization of the brain has been one of the biggest challenges of the last century and to this day developing a map of its complex structure is a central goal of contemporary neuroscience (Sporns, 2015). Among the in vivo techniques for neuroimaging based on magnetic resonance imaging (MRI), diffusion-weighted imaging (DWI) has become an essential tool for the characterisation of white matter at both, the micro-scale by supporting the development of a number of microstructural imaging techniques, and the macro-scale, by enabling white matter pathways to be reconstructed thus mapping brain connections.

In the area of microstructural imaging, DWI has enabled the development of mathematical models that characterize the complex tissue of the brain at a scale beyond the MRI native resolution (Duval et al., 2016). One popular example is neurite orientation dispersion and density imaging (NODDI), which estimates neurite morphological indices by means of multi-shell diffusion imaging and compartmental modelling (Zhang et al., 2012). Combining the obtained microstructural information with other non-conventional MRI methods such as quantitative magnetization transfer (MT) imaging allows an even more detailed characterization of the underlying cellular structure, estimating the myelin distribution in terms of the g-ratio, which is the ratio between the inner and the outer diameter of the myelinated axon (Stikov et al., 2015). Notably, myelination is a key feature for the rapid signal propagation needed by motory, sensory and cognitive functions (Nave and Werner, 2014), and measuring it in vivo allows further insights in the understanding of plasticity, aging and neuroinflammation.

At the macro-scale, DWI has been paramount for connectomics: the estimation of the connectome, the map made of neural elements and their connections (Sporns et al., 2005; Hagmann, 2005), has become viable at the macroscale only by means of DWI and

tractography, i.e. the reconstruction of white matter streamlines (Basser et al., 2000). Inheriting its fundamentals from network science, this approach offers an elegant model to describe a complex system such as the brain by means of a mathematical graph, reducing the characterization of a map of the brain to the analysis of its topological features (Bullmore and Sporns, 2009). This approach has shed light not only on several aspects of the brain organization (Collin et al., 2014), but also on potential mechanisms of brain disorders (Fornito et al., 2015; van den Heuvel et al., 2013). In particular, the presence of hub regions highly interconnected with each other has been observed, forming the so-called rich-club (van den Heuvel and Sporns, 2011). It is important to keep in mind that these studies heavily rely on the streamlines reconstructed by means of tractography and typically use the total number of streamlines connecting a pair of nodes as a measure of their connectivity. Such an approach has some limitations related to false positives detection and inaccurate streamlines termination (Maier-Hein et al., 2016). The combination of tractographic reconstruction with microstructural imaging techniques has been proposed as a possible way to improve it (Daducci et al., 2016; van den Heuvel and Yeo, 2017).

The advantages of this combination can work in two complementary directions. On the one hand, the integration of microstructural properties in a network model can lead to a more complete picture of the brain structure (Knösche1 and Tittgemeyer, 2011). Recent works have attempted this by fusing together structural connectivity with NODDI and qMT data in multiple sclerosis and epilepsy (Lemkaddem et al., 2014; Mancini et al., 2016; Pardini et al., 2015), using microstructural measures to weight the estimated structural networks. On the other hand, tractography algorithms can be improved by taking into account microstructural information. An interesting example is given by microstructure informed tractography (Daducci et al., 2015), which combines tractography and tissue microstructure using a convex optimization approach.

In this paper, we focus on the former of these two perspectives. We propose to integrate myelination measures in the connectome by means of weighting the graph edges using the g-ratio. The rationale for this is that the g-ratio is believed to be proportional to the axonal speed of conduction, and therefore it may be used to characterize the efficiency of any given connection. To achieve this goal, we first reconstructed the connectome using the number of streamlines as done in the current literature for two different datasets of healthy subjects. Then, we integrated the g-ratio after the reconstruction process and we compared the resulting properties with more conventional measures of structural connectivity, with the aim of characterizing the connectome taking into account myelination. Our hypothesis was that the g-ratio would show complementary aspects when looking at the global picture while highlighting specific levels of organization in more details.

2. Materials and Methods

2.1 Data acquisition

Two datasets were analysed for the purpose of validating the results by comparison. The principal dataset included 16 subjects and was collected at the Clinical Imaging Sciences Centre, Brighton and Sussex Medical School, Brighton (site A), using a 1.5T Siemens Magnetom Avanto. The replication dataset included 15 subjects and was collected at the Neuroimaging Laboratory, Santa Lucia Foundation, Rome (site B), using a 3T Philips Achieva. The data were acquired as part of two studies approved, respectively, by the Herefordshire and the Santa Lucia Foundation Research Ethics Committee. Details about the two populations are available in the supplementary materials.

2.1.1 Principal dataset

At site A, 16 healthy subjects (M/F: 6/10; mean age (SD): 25 (6.2)) were scanned using the 32-channel head coil for signal reception and the body coil for transmission. The protocol included: a magnetisation prepared rapid gradient echo (MPRAGE) sequence (TR=2730 ms, TE=3.57 ms, TI=1000 ms, flip angle=7°, matrix=256x240x192, slice thickness=1 mm, FoV=256x240 mm^2); 3-shell DWI sequence for NODDI (TE=99 ms, TR=8400 ms, matrix=96x96, FoV=240x240 mm^2, slice thickness = 2.5 mm, 10 b0 volumes; 9 directions with b=300 smm^{-2}; 30 directions with b=800 smm^{-2}; 60 diffusion directions with b=2400 smm^{-2}); quantitative MT imaging based on balanced steady-state free precession (bSSFP) using a 3D True Fast Imaging with Steady-state precession (TrueFisp) sequence and 3D fast low-angle shot (FLASH) volumes for T1-mapping (field of view (FOV)=240x180 mm^2; matrix=256x96; slices=32; slice thickness=5 mm).

2.1.2 Replication dataset

At site B, images from 15 healthy subjects (M/F: 7/8; mean age (SD): 28.9 (4.8)) were acquired using a 32-channel head coil. The procedure involved: a 3D T1 fast field echo (FFE) sequence (TR=11 ms, TE=5.3 ms, flip angle=8°, matrix=256x228x190, slice thickness=0.9 mm, FOV=230x192x167 mm^3); a multi-shell high angular resolution diffusion imaging (HARDI) scheme, optimized for NODDI protocol (TR= 12.5 s, TE= 91 ms, isotropic resolution= 2.3 mm^3, 9 b0 volumes; first shell: 30 gradient directions, b=711 smm^{-2}; second shell: 60 directions, b=2855 smm^{-2}); a series of 12 MT-weighted FLASH sequences (TE=7.4 ms, TR=35 ms, flip angle=7°, matrix=128x96x28, FOV=230x172.5x140 mm^3) with variable flip angle and offset frequency of the Gaussian MT pulses (Giulietti et al., 2012); three 3D FLASH sequences collected for mapping the observed T1 of the system (TE=4.8 ms, TR=15 ms, flip angles=5°, 7°, 15°, same matrix and FOV as the MT sequence); three 3D FLASH sequences collected for B1 mapping (TE=4.8 ms, TR=28 ms, flip angles=155°, 180°, 205°, matrix=64x64x40, FOV=220x220x160 mm^3).

2.2 Anatomical and diffusion data pre-processing

The processing pipeline used to obtain the connectivity matrices from the data is briefly illustrated in figure 1. T1 images were pre-processed using FreeSurfer for grey/white matter tissue classification and parcellation by means of the Desikan-Killiany atlas, obtaining 14 subcortical and 68 cortical regions (Desikan et al., 2006). Diffusion data were first co-registered to the respective average of b_0 volumes in order to minimize artifacts (Cercignani et al., 2012). Then, streamlines were deterministically reconstructed using tensor fitting and the fiber assignment by continuous tracking (FACT) algorithm (Mori et al., 1999) by means of Diffusion Toolkit (Wang et al., 2007). In particular, for every voxel within the grey matter tissue mask, streamlines within the white matter tissue mask were started from eight seeds and terminated when the trajectory either entered in a voxel with a fractional anisotropy (FA) less than 0.1 or made a turn sharper than 45º. The number of seeds, randomly distributed within the voxel, was chosen as a trade-off between reducing network variance and avoiding spurious results (Cheng et al., 2012). Streamlines with origins in grey matter tissue mask that exceeded the white matter tissue mask were discarded. An additional set of streamlines was obtained using more conservative thresholds (FA threshold=0.2; degree threshold=30º). The reconstructed streamlines were then co-registered to the anatomical space using an inverse linear transformation estimated using FSL FLIRT.

Please insert Figure 1 about here

2.3 Parametric maps and g-ratio estimation

Quantitative MT data for both sites were analysed using in-house software in order to estimate the macromolecular proton pool size ratio (F) voxel-wise. First, all the MT-weighted volumes (bSSFP for site A and FLASH for site B) and T1 mapping volumes were spatially realigned to the 25° flip angle FLASH volume using rigid-body registration by means of FSL FLIRT (Jenkinson et al., 2002). T1 maps were obtained by fitting the 3 FLASH volumes to theoretical voxel values for the spoiled gradient echo for the three flip angles (Venkatesan et al., 1998). The MT parameters were then obtained by performing a voxel-wise nonlinear least-squares fitting (Levenberg-Marquardt method) to the appropriate binary spin bath model: Gloor's model (Gloor et al., 2008) for site A, and Ramani's (Ramani et al., 2007) model for site B.

Multi-shell diffusion data were analysed using either the NODDI (site A) or the AMICO (site B) toolboxes (Zhang et al., 2012; Daducci et al., 2015) to compute the intra-cellular water compartment and the isotropic component volume maps (v_{ic} and v_{iso} respectively). Then, MT and NODDI data were non-linearly co-registered using ANTs to a common MNI space.

Maps of the aggregate g-ratio were obtained as described by Stikov and colleagues (Stikov et al., 2015). From the maps, the g-ratio was computed assuming that the g-ratio is constant within the voxel, using the equation:

$$g = \sqrt{1 - \frac{MVF}{FVF}} = \sqrt{\left(1 + \frac{MVF}{AVF}\right)^{-1}} \quad (1)$$

where g is the g-ratio, MVF is the myelin volume fraction, FVF is the fiber volume fraction, and AVF is the axon volume fraction (Stikov et al., 2015). According to this model, MVF can be derived from any MRI modality that is sensitive to myelin. Following Stikov et al, we used the pool size ratio, F, derived from quantitative MT.

We then set:

$$MVF = kF \quad (2)$$

where k is a proportionality constant not known a priori, which was derived using a simple approach already described in previous works (Cercignani et al., 2016; Cercignani et al., 2017). Briefly, using the JHU white-matter tractography atlas (available with FSL) the unbiased masks of the forceps major and minor were extracted for the F, v_{ic} and v_{iso} maps (appropriately co-registered to the JHU template). The g-ratio values estimated from these maps were evaluated as a function of k in order to identify the value corresponding to g-ratio≈0.7. The procedure was repeated independently for the 2 datasets.

AVF can be derived from the intracellular volume fraction estimated from NODDI (v_{ic}), adjusted for MVF and for the volume of the isotropic component of diffusion (v_{iso} – also derived from NODDI) (Stikov et al, 2015).

$$AVF = (1 - MVF)(1 - v_{iso})v_{ic} \quad (3)$$

MVF and AVF were computed voxel-wise and then used to estimate the g-ratio maps. These were finally co-registered to the anatomical space using an inverse non-linear warping. Further details on the g-ratio computation can be found elsewhere (Cercignani et al., 2017).

2.4 Connectome reconstruction

2.4.1 Structural brain networks

Structural networks were modelled by means of weighted graphs, where n nodes are connected by unique edges and each edge has a weight associated that reflects its strength. The structural connectome was reconstructed for each subject counting the number of

streamlines (NOS) between every possible pair of regions, and arranging such values into an adjacency matrix. We used the set of streamlines estimated for the less conservative thresholds (FA threshold=0.1; degree threshold=45º) and checked for the absence of substantial differences when using the stricter ones. We assessed the presence of outliers in both datasets using a simple approach based on the interquartile range. Briefly, for each subject we calculated the average number of streamlines, the average FA and g-ratio values, and the prevalence of connections and disconnections. For each of those measures, we calculated the first and the third quartile as well as the interquartile range (respectively Q_1, Q_3 and IQR) and used Q_1-1.5·IQR and Q_3+1.5·IQR as thresholds for identifying outliers.

In order to avoid spurious connections, we considered as connected only regions with at least two estimated streamlines between them, and we used more conservative thresholds (at least four and at least six streamlines) to test how robust the results were. Furthermore, to avoid false positives, we selected only the edges present in at least 50% of the subjects of each dataset (de Reus and van den Heuvel, 2013). NOS-based strength distribution for all the regions was computed in order to characterize the structural networks. We then looked at the hub organization: hubs have been defined as the eight regions with the highest strength values in line with the literature (van den Heuvel and Sporns, 2013), using therefore NOS measures as weights. To assure the reliability of the results, we repeated our analysis using alternative hub definitions. In particular, we defined hub regions first considering the top twelve regions in terms of strength (instead of the top eight), and then as a further criterion we selected regions with strength greater than the average plus one standard deviation. The connections have been then classified on the basis of the nodes interconnected and in light of the estimated hub structure (connection between two hub regions: rich-club (RC); connection between a hub region and a peripheral one: feeder (FD); connection between two peripheral regions: local (LC)). In this way, we were able to characterize the hub organization without

focusing specifically on hub-hub connections (van den Heuvel et al., 2013). The classification has been repeated for all the hub definition criteria for reliability purposes. In order to take into account different perspectives, other classification criteria were explored: the connections were classified on the basis of the subcortico-cortical (subcortical (SUB); subcortico-cortical (SC); cortico-cortical (CORT)) and the inter-/intra-hemispherical (intra-hemispheric, left; intra-hemispheric, right; inter-hemispheric) organization levels.

2.4.2 G-ratio weighted networks

G-ratio weighted networks were modelled using a slightly different approach. Rather than using the average g-ratio of the streamlines between a given pair of regions, the g-ratio values for all the streamlines were taken into account, modelling the network as a multigraph (Shafie, 2015), where multiple edges (instead of a single one) connect the nodes (one for each streamline), and every edge has its own weight, in this case the g-ratio itself. Although it may sound cumbersome, this approach is naturally sound for brain structural connectivity, since it gives us the chance of characterising individually the different white matter fibers estimated between a given pair of regions. This choice was mainly due to avoid biased results as in the Simpson's paradox (Kievit et al., 2013): using a multigraph, the average weight (e.g. the g-ratio) of a node's connections is given by the mean of all the weights of its streamlines rather than subdividing those streamlines by specific pairs of regions.

However, it must be kept in mind that the aim of this paper is the characterization of the g-ratio weighted network in relation to the NOS-weighted structural network. The characterization of the g-ratio distribution will be then given in terms of average across connection classes and brain regions, avoiding further assumptions on concepts such as distance and motifs. As a result, the use of such model will not present any further difference compared to simple graph-based approaches.

As a first characterization, we calculated for each region the average g-ratio for all the connected streamlines and compared it to NOS-weighted strength distribution. As a second step, we sorted the obtained average g-ratio distribution in ascending order, since given the axon diameter the g-ratio is inversely proportional to the myelin volume and also to the electrostatic energy cost (Paus et al., 2014). Then, for each connection class previously identified, we calculated the median of the related g-ratio distribution. For each classification criteria, we tested the median values to identify significant differences. Sign test was used for assessing the significance of the difference between connection classes, therefore testing non-parametrically the hypothesis that the difference between each pair of classes had zero median under the assumption of continuous distributions (Whitley and Ball, 2002). Given the number of comparisons performed (three for each classification criterion, three classification criteria) and in order to avoid the multiple comparisons problem, we corrected the p-values with the Bonferroni correction as appropriate. In order to show further elements of the hub structure, we used the s-core decomposition (van den Heuvel and Sporns, 2011): for an increasing range of strength thresholds, the connections with a lower strength value were removed and the median g-ratio of remaining streamlines was computed.

2.4.3 Additional analyses

In order to provide further elements to characterize the datasets in terms of NOS distributions, we compared the connection classes in the NOS-weighted networks and provided for comparison purposes a brief characterization for FA-weighted networks. Moreover, for further assessments of relationship between the NOS- and G-ratio-weighted networks, we examined the correlation of those networks and characterised them as a function of the streamline length. Details about these additional methods and the related results are available in the supplementary materials.

3. Results

Good quality g-ratio maps were obtained for all participants. The scaling factors k were, respectively, 2.4 and 2.5 for sites A and B. Figure 2 shows the networks respectively reconstructed using NOS and g-ratio values and the histogram of the g-ratio distribution for the reconstructed streamlines, averaged over the subjects. Apart from some differences in terms of number of reconstructed tracts, it can be observed that the most frequent g-ratio value is 0.76 for the main dataset and 0.71 for the replication one.

Please insert Figure 2 about here

As expected, the strength distribution in terms of NOS for both the datasets shows the trend of a power law distribution (figure 3). Among the nodes with the highest strength, there are the superior frontal gyrus, the precentral one, the superior parietal gyrus (dataset A) and the putamen (dataset B). The corresponding average g-ratio distribution does not follow the same trend. Sorting such distribution by ascending g-ratio values, the regions with the lowest values in both datasets are given by the precentral and the paracentral gyri as well as the superior frontal gyrus.

Please insert Figure 3 about here

ACCEPTED MANUSCRIPT

In terms of the hub structure, there is a significant trend which is consistent in both the datasets (figure 4): the rich-club and feeder connections show a significantly lower g-ratio than the local ones (dataset A, RC-LC: p_{corr}=0.036; FD-LC: p_{corr} =0.0027; dataset B, RC-LC: p_{corr}=0.00054; FD-LC: p_{corr}=0.00054). Although the rich-club connections show also a significantly lower g-ratio than the feeder ones in the replication dataset, this result is not consistent with the main dataset (dataset A, RC-FD: p_{corr} =0.18; dataset B, RC-FD: p_{corr} =0.0081). As a further confirmation of this trend, the median g-ratio decreases as the strength increases in the s-core decomposition in both the datasets.

From the subcortico-cortical point of view, in both the datasets there are significant differences comparing all the connection classes (dataset A, SUB-SC: p_{corr}=0.00027; SUB-CORT: p_{corr}=0.0045; SC-CORT: p_{corr}=0.00027; dataset B: SUB-SC: p_{corr}=0.00054; SUB-CORT: p_{corr}=0.00054; SC-CORT: p_{corr}=0.00054). However, while the subcortical connections showed consistently and significantly higher values than the others in both the datasets, subcortico-cortical and cortical connections gave conflicting results when comparing the 2 datasets.

Finally, from the inter-intrahemispheric point of view, again in both the datasets there are several significant differences comparing the connection classes, with the intrahemispheric connections of the left hemisphere showing consistently a higher g-ratio than the others (dataset A, L-I: p_{corr}=0.00027; L-R p_{corr}=0.00027; dataset B, L-I: p_{corr}=0.00054; L-R: p_{corr}=0.00054). The other comparisons did not match between the main and the replication datasets (dataset A, I-R: p_{corr}=0.63; dataset B, I-R: p_{corr}=0.0081).

Further details on the results as well as individual data for the subjects are available in the supplementary materials.

Please insert Figure 4 about here

4. Discussion

In this paper, we proposed the integration of the connectome with myelin content measures using network modelling and g-ratio computation. Since the white matter is practically a transport system (Paus et al., 2014), in order to assess its structure and function it is necessary to have information about the transport processes in terms of speed and delay. Therefore, we characterized NOS-weighted structural connectivity with the related g-ratio data in two different datasets in order to describe the myelinated connectome in healthy subjects.

Our results can be summed up in three points: first, the average g-ratio for the connections of each region does not follow the trend of the related strength distribution; second, a myelin blueprint can be observed looking at the hub structure; third, the anatomical organization follows patterns consistent with existing literature.

Several papers in the last years have started characterizing the g-ratio distribution in vivo using MRI (Campbell et al., 2017), both in the healthy adult (Cercignani et al., 2017; Mohammadi et al., 2015) and developing brains (Dean et al., 2016; Melbourne et al., 2016). To the best of our knowledge, this is the first attempt to characterize the variability of this measure in the streamlines used to reconstruct the connectome. As a first step, then, we have focused on the strength distribution used to characterize most real-world networks and compared it to the average g-ratio of each node. As clear from figure 3, the g-ratio distribution does not resemble the strength one. However, sorting the distribution by ascending g-ratio values, the regions with lower g-ratio and therefore with higher myelin proportion are the ones involved in motor and somatosensory functions as one would expect

(Nave and Werner, 2014). This observation confirms the fact that the g-ratio can provide complementary information to that provided by tractography, generating interesting perspectives for the study of structure-function coupling.

A second important result is that the rich-club and feeder connections have significantly lower g-ratio values than local connections, suggesting that the connections that involve the hubs have higher myelin content than the others. A preliminary result by Collin and colleagues showed a similar trend using magnetization transfer ratio while taking into account only a reduced number of hubs and only in terms of hub-hub connections (Collin et al., 2014). Using the g-ratio, we were able to see a more general trend in both datasets involving all the hub connections, both the ones with other hubs and the ones with peripheral regions, and using different hub definition criteria. As a consequence, rich-club and feeder connections are capable of faster and more efficient propagation than the local ones. At the same time, the energetic cost for oligodendrocytes maintenance outweighs savings in propagation (Harris and Attwell, 2012), making the higher myelin content another one of the high-cost features of the brain (Collin et al., 2014; van den Heuvel and Sporns, 2013).

Regarding anatomical classifications, the subcortico-cortical results suggest less myelinated fibers between the subcortical structures than in the cortical case. This result is consistent with g-ratio values measured in rats, where the axons connecting the brainstem and the internal capsule showed higher g-ratio than the ones in the anterior commissure and the corpus callosum (Chomiak and Hu, 2009). Instead, the inter-intrahemispheric results show a less clear picture, although confirming the idea of asymmetry between the hemispheres (Cercignani et al., 2017). It must be noticed that the largest commissural fiber bundle, the corpus callosum, contains axons of variable calibers. In particular, those in the splenium are known to have very large diameter and thin myelin sheath (Hildebrand and Hahn, 1978;

Stikov et al., 2015). In light of this observation, characterizing interhemispheric streamlines as a whole may offer a too general view that is not consistent and hard to interpret.

It is worth having a deeper look at comparison of the g-ratio with other possible weights for a network. The NOS-weighted results included in the supplementary materials showed good agreement with previous literature (van den Heuvel and Sporns, 2011; Collin et al., 2014) but they were not indicative of the ones based on g-ratio. When looking at the correlation between NOS and g-ratio, the relationship was rather modest and the related plot qualitatively different from a linear relationship. Examining the possible relationships with the fiber lengths, we did not again observe strong relationships using neither the g-ratio or the NOS as a weight. In the latter case, we could in any case distinguish differences in light of the hub structure. As a further analysis, we used FA-weighted networks as an additional comparison. Although we obtained trends comparable with the ones previously described (Collin et al., 2014), we did not observe shared patterns with the g-ratio-weighted ones (as detailed in the supplementary materials). This result highlights how the g-ratio do not rely only on diffusion-based measures and that the use of both magnetization and diffusion data is necessary for the chosen model.

These results could serve as a starting point for investigating other scenarios. The potential applications of this approach span several topics. The first one is the study of plasticity mechanisms beyond synaptic ones: one of these mechanisms is believed to rely on the possibility of changing conduction velocity through changes in myelin (Fields, 2015; Seidl, 2014; Wang and Young, 2014). In this context, a study on rats showed that an enriched environment induces significant increases in terms of myelin content compared to a standard one (Yang et al., 2013). Promisingly, estimating the g-ratio in vivo and observing it through the lenses of connectomics could lead to new insights on activity-dependent myelination in humans.

A further perspective related to plasticity is non-invasive brain stimulation: recent works have used network modelling to investigate the mechanisms of transcranial magnetic stimulation (TMS) given the structural connectivity and the stimulation site (Cocchi et al., 2016; Gollo et al., 2017). This approach has provided interesting insights in how brain dynamics respond to focal perturbations that could be extended integrating the g-ratio.

Another important application would be the study of neuroinflammation, with a special focus on multiple sclerosis (MS), where demyelination and remyelination phenomena are key elements to evaluate pathophysiology and the response to treatment. A few studies have given a glimpse of the possible application in particular looking at the g-ratio in lesion sites (Cercignani et al., 2015; Stikov et al., 2015). However, it would certainly be interesting to investigate whole-brain potential early signs of the disease evolution. In any case, attention should be paid to some challenging issues while estimating the g-ratio in MS (Campbell et al., 2017; Stikov et al., 2015).

Despite all the potential applications, it is necessary to briefly present some methodological points as well as some limitations of this work. An important choice in network modelling regards how to weight the connections between elements (Fornito et al., 2016). In this work, we used the g-ratio value as estimated from NODDI and qMT data in order to provide a straightforward reference for future studies. Although it would be tempting to obtain and use directly conduction velocity as a weight, there are several elements that need to be taken into thorough consideration (Fornito et al., 2013).

The first point is the mathematical expression of conduction velocity itself as a function of the g-ratio. For the peripheral nervous system (PNS), such an expression has been clearly defined and some papers used it for the central nervous system (CNS) as well (Melbourne et al., 2014). However, it is known that such an expression needs to be adjusted because of the

different physical aspects of the brain compared to peripheral nerves (Chomiak and Hu, 2009; Pajevic and Basser, 2013). Indeed, it is important to be careful with computing the conduction velocity: as shown in a computational work (Pajevic et al., 2014), small changes in its value can have profound effects on neural activity in terms of synchrony and signal propagation. This consideration leads to an important issue: in order to properly estimate the conduction velocity in the CNS, it is necessary to have an estimate of the diameter of the fibers (Chomiak and Hu, 2009). Such information has been measured ex-vivo for specific bundles and there are some attempts to estimate it in vivo for the corpus callosum (Barazany et al., 2009), but its integration in the described network model goes beyond the scope of this work.

Another element worth mentioning is the choice of network measures. In this paper, in order to compare the g-ratio weighted networks with the NOS weighted ones we restricted our analysis to average and median values of the tracts of interest and used classification criteria based on NOS and anatomy to characterize the connections in terms of g-ratio. We did not calculate canonical measures such as the clustering coefficient and the path length for the sake of interpretability: these measures rely on the assumption that the connections are weighted proportionally to their information transfer capability. In the case of the g-ratio, the relationship with information transfer is not straightforward, since neither directly or inversely proportional to it. Again, using conduction velocity as a weight would certainly allow to use and interpret properly more measures inherited from graph theory. However, as already pointed out, the estimation of the conduction velocity in the CNS requires knowledge about both the g-ratio and the axonal diameter. Without knowing the axonal diameter, the g-ratio itself does not offer clear information for the definition of distance and motifs in a network.

This work has also some limitations. Estimating the g-ratio relies in first instance on the assumption that its value is constant within the voxel. However, these results could be tested using approaches that do not rely on this assumption (West et al., 2016) or in light of the recent observations on FA (Chang et al., 2017). Another aspect to take into account is that since the g-ratio estimation relies on qMT and NODDI, it inherits all the pitfalls of these modalities in terms of assumptions and errors. In particular, while F has been shown to correlate with myelination (as in Turati et al., 2015), MT is also sensitive to other factors, such as oedema, inflammation and pH (Stanisz et al., 2004, Vavasour et al., 2011). In addition, the proportionality between MVF and F is established through an empirical procedure which may be seen as arbitrary. It is important to reiterate that a wrong calibration could lead to the computed g-ratio having some dependency on FVF (Campbell et al., 2017). The consequences of this on topological measures derived from graph theory remain to be explored. Finally, the values of v_{ic} and v_{iso} used to compute AVF are derived from NODDI, which makes some strong assumptions about the intracellular diffusivity which do not always hold true (Lampinen et al., 2017).

A further limitation lies in the connectome estimation: it has been shown that using diffusion data to estimate the connectome inevitably leads to false positive (Maier-Hein et al., 2016). This is an issue mainly of reconstruction algorithms and to this day there are no other viable solutions to avoid this problem.

We used two distinct datasets to cross-validate our findings. While overall the main results are replicable between datasets, there are of course some important differences that deserve discussing. First, there seems to be a systematic difference in the most represented g-ratio between A and B. It is possible that this is a consequence of procedure used to calibrate the factor k. k can vary depending on the specific MT method or model used (Stikov et al., 2015; Campbell et al., 2017) and ideally requires histological validation. We should reiterate,

however, that the data were collected at different field strengths, and using very different MT acquisitions and modelling, and the effects of noise and field uniformity are expected to affect g-ratio measurement.

Despite this, most of the results on the properties of g-ratio-weighted graphs show good agreement overall between the two datasets. This suggests that g-ratio computation is robust enough for more applications in experimental studies.

ACCEPTED MANUSCRIPT

References

Barazany, D., Basser, P.J., Assaf, Y., 2009. In vivo measurement of axon diameter distribution in the corpus callosum of rat brain. Brain 132(5): 1210-1220.

Basser, P.J., Pajevic, S., Pierpaoli, C., Duda, J., Aldroubi, A., 2000. In vivo fiber tractography using DT-MRI data. Magn Reson Med 44, 625-632.

Bullmore, E., Sporns, O., 2009. Complex brain networks: graph theoretical analysis of structural and functional systems. Nat Rev Neurosci 10, 186-198.

Campbell, J.S., Leppert, I.R., Narayanan, S., Duval, T., Cohen-Adad, J., Pike, G.B., Stikov, N., 2017. Promise and pitfalls of g-ratio estimation with MRI. arXiv preprint arXiv:1701.02760.

Cercignani, M., Embleton, K., Parker, G.J., Bozzali, M., 2012. Group-averaged anatomical connectivity mapping for improved human white matter pathway visualisation. NMR Biomed 25, 1224-1233.

Cercignani, M., Giulietti, G., Dowell, N., Spano, B., Harrison, N., Bozzali, M., 2016. A simple method to scale the macromolecular pool size ratio for computing the g-ratio in vivo. ISMRM Annual Meeting, Singapore.

Cercignani, M., Giulietti, G., Dowell, N.G., Gabel, M., Broad, R., Leigh, P.N., Harrison, N.A., Bozzali, M., 2017. Characterizing axonal myelination within the healthy population: a tract-by-tract mapping of effects of age and gender on the fiber g-ratio. Neurobiol Aging 49, 109-118.

Cercignani, M., Giulietti, G., Spanò, B., Bozzali, M., 2015. Mapping the g-ratio within MS lesions. ISMRM Annual Meeting, Toronto.

Cheng, H., Wang, Y., Sheng, J., Sporns, O., Kronenberger, W.G., Mathews, V.P., Hummer, T.A., Saykin, A.J., 2012. Optimization of seed density in DTI tractography for structural networks. J Neuroscience Meth 203(1): 264-272.

Chang, E.H., Argyelan, M., Aggarwal, M., Chandon, T.S., Karlsgodt, K.H., Mori, S., Malhotra, A.K., 2017. The role of myelination in measures of white matter integrity: Combination of diffusion tensor imaging and two-photon microscopy of CLARITY intact brains. Neuroimage 147, 253-261.

Chomiak, T., Hu, B., 2009. What is the optimal value of the g-ratio for myelinated fibers in the rat CNS? A theoretical approach. PLoS One 4, e7754.

Cocchi, L., Sale, M.V., L, L.G., Bell, P.T., Nguyen, V.T., Zalesky, A., Breakspear, M., Mattingley, J.B., 2016. A hierarchy of timescales explains distinct effects of local inhibition of primary visual cortex and frontal eye fields. Elife 5.

Collin, G., Sporns, O., Mandl, R.C., van den Heuvel, M.P., 2014. Structural and functional aspects relating to cost and benefit of rich club organization in the human cerebral cortex. Cereb Cortex 24, 2258-2267.

Daducci, A., Canales-Rodriguez, E.J., Zhang, H., Dyrby, T.B., Alexander, D.C., Thiran, J.P., 2015. Accelerated Microstructure Imaging via Convex Optimization (AMICO) from diffusion MRI data. Neuroimage 105, 32-44.

Daducci, A., Dal Palu, A., Descoteaux, M., Thiran, J.P., 2016. Microstructure Informed Tractography: Pitfalls and Open Challenges. Front Neurosci 10, 247.

Daducci, A., Dal Palu, A., Lemkaddem, A., Thiran, J.P., 2015. COMMIT: Convex optimization modeling for microstructure informed tractography. IEEE Trans Med Imaging 34, 246-257.

de Reus, M.A., van den Heuvel, M.P., 2013. Estimating false positives and negatives in brain networks. Neuroimage 70, 402-409.

Dean, D.C., 3rd, O'Muircheartaigh, J., Dirks, H., Travers, B.G., Adluru, N., Alexander, A.L., Deoni, S.C., 2016. Mapping an index of the myelin g-ratio in infants using magnetic resonance imaging. Neuroimage 132, 225-237.

Desikan, R.S., Segonne, F., Fischl, B., Quinn, B.T., Dickerson, B.C., Blacker, D., Buckner, R.L., Dale, A.M., Maguire, R.P., Hyman, B.T., Albert, M.S., Killiany, R.J., 2006. An automated labeling system for subdividing the human cerebral cortex on MRI scans into gyral based regions of interest. Neuroimage 31, 968-980.

Duval, T., Stikov, N., Cohen-Adad, J., 2016. Modeling white matter microstructure. Funct Neurol 31, 217-228.

Fields, R.D., 2015. A new mechanism of nervous system plasticity: activity-dependent myelination. Nat Rev Neurosci 16, 756-767.

Fornito, A., Zalesky, A., Breakspear, M., 2013. Graph analysis of the human connectome: promise, progress, and pitfalls. Neuroimage 80, 426-444.

Fornito, A., Zalesky, A., Breakspear, M., 2015. The connectomics of brain disorders. Nat Rev Neurosci 16, 159-172.

Fornito, A., Zalesky, A., Bullmore, E., 2016. Fundamentals of Brain Network Analysis. Elsevier Science.

Giulietti, G., Bozzali, M., Figura, V., Spano, B., Perri, R., Marra, C., Lacidogna, G., Giubilei, F., Caltagirone, C., Cercignani, M., 2012. Quantitative magnetization transfer

provides information complementary to grey matter atrophy in Alzheimer's disease brains. Neuroimage 59, 1114-1122.

Gloor, M., Scheffler, K., Bieri, O., 2008. Quantitative magnetization transfer imaging using balanced SSFP. Magn Reson Med 60, 691-700.

Gollo, L.L., Roberts, J.A., Cocchi, L., 2017. Mapping how local perturbations influence systems-level brain dynamics. Neuroimage.

Hagmann, P., 2005. From diffusion MRI to brain connectomics. EPFL.

Harris, J.J., Attwell, D., 2012. The energetics of CNS white matter. J Neurosci 32, 356-371.

Hildebrand, C., Hahn, R., 1978. Relation between myelin sheath thickness and axon size in spinal cord white matter of some vertebrate species. J Neurol Sci 38, 421-434.

Jenkinson, M., Bannister, P., Brady, M., Smith, S., 2002. Improved optimization for the robust and accurate linear registration and motion correction of brain images. Neuroimage 17, 825-841.

Kievit, R.A., Frankenhius, W.E., Waldorp, L.J., Borsboom, D., 2013. Simpson's paradox in psychological science: a practical guide. Front Psychol 4: 513.

Knosche, T.R., Tittgemeyer, M., 2011. The role of long-range connectivity for the characterization of the functional-anatomical organization of the cortex. Front Syst Neurosci 5, 58.

Lampinen, B., Szczepankiewicz, F., Mårtensson, J., van Westen, D., Sundgren, P.C., Nilsson, M., 2017. Neurite density imaging versus imaging of microscopic anisotropy in

diffusion MRI: A model comparison using spherical tensor encoding. Neuroimage 147, 517-531.

Lemkaddem, A., Daducci, A., Kunz, N., Lazeyras, F., Seeck, M., Thiran, J.P., Vulliemoz, S., 2014. Connectivity and tissue microstructural alterations in right and left temporal lobe epilepsy revealed by diffusion spectrum imaging. Neuroimage Clin 5, 349-358.

Maier-Hein, K., Neher, P., Houde, J.-C., Cote, M.-A., Garyfallidis, E., Zhong, J., Chamberland, M., Yeh, F.-C., Lin, Y.C., Ji, Q., 2016. Tractography-based connectomes are dominated by false-positive connections. bioRxiv, 084137.

Mancini, M., Giulietti, G., Spano, B., Bozzali, M., Cercignani, M., Conforto, S., 2016. Estimating multimodal brain connectivity in multiple sclerosis: an exploratory factor analysis. Conf Proc IEEE Eng Med Biol Soc 2016, 1131-1134.

Melbourne, A., Eaton-Rosen, Z., Orasanu, E., Price, D., Bainbridge, A., Cardoso, M.J., Kendall, G.S., Robertson, N.J., Marlow, N., Ourselin, S., 2016. Longitudinal development in the preterm thalamus and posterior white matter: MRI correlations between diffusion weighted imaging and T2 relaxometry. Hum Brain Mapp 37, 2479-2492.

Mohammadi, S., Carey, D., Dick, F., Diedrichsen, J., Sereno, M.I., Reisert, M., Callaghan, M.F., Weiskopf, N., 2015. Whole-Brain In-vivo Measurements of the Axonal G-Ratio in a Group of 37 Healthy Volunteers. Front Neurosci 9, 441.

Mori, S., Crain, B.J., Chacko, V.P., van Zijl, P.C., 1999. Three-dimensional tracking of axonal projections in the brain by magnetic resonance imaging. Ann Neurol 45, 265-269.

Nave, K.A., Werner, H.B., 2014. Myelination of the nervous system: mechanisms and functions. Annu Rev Cell Dev Biol 30, 503-533.

Pajevic, S., Basser, P.J., 2013. An optimum principle predicts the distribution of axon diameters in normal white matter. PLoS One 8, e54095.

Pajevic, S., Basser, P.J., Fields, R.D., 2014. Role of myelin plasticity in oscillations and synchrony of neuronal activity. Neuroscience 276, 135-147.

Pardini, M., Yaldizli, O., Sethi, V., Muhlert, N., Liu, Z., Samson, R.S., Altmann, D.R., Ron, M.A., Wheeler-Kingshott, C.A., Miller, D.H., Chard, D.T., 2015. Motor network efficiency and disability in multiple sclerosis. Neurology 85, 1115-1122.

Paus, T., Pesaresi, M., French, L., 2014. White matter as a transport system. Neuroscience 276, 117-125.

Ramani, A., Dalton, C., Miller, D.H., Tofts, P.S., Barker, G.J., 2002. Precise estimate of fundamental in-vivo MT parameters in human brain in clinically feasible times. Magn Reson Imaging 20, 721-731.

Seidl, A.H., 2014. Regulation of conduction time along axons. Neuroscience 276, 126-134.

Shafie, T., 2015. A Multigraph Approach to Social Network Analysis. Journal of Social Structure 16.

Sporns, O., 2015. Cerebral cartography and connectomics. Philos Trans R Soc Lond B Biol Sci 370.

Sporns, O., Tononi, G., Kotter, R., 2005. The human connectome: A structural description of the human brain. PLoS Comput Biol 1, e42.

ACCEPTED MANUSCRIPT

Stanisz, G.J., Webb, S., Munro, C.A., Pun, T., Midha, R., 2004. MR properties of excised neural tissue following experimentally induced inflammation. Magn Reson Med. 51: 473–479.

Stikov, N., Campbell, J.S., Stroh, T., Lavelee, M., Frey, S., Novek, J., Nuara, S., Ho, M.K., Bedell, B.J., Dougherty, R.F., Leppert, I.R., Boudreau, M., Narayanan, S., Duval, T., Cohen-Adad, J., Picard, P.A., Gasecka, A., Cote, D., Pike, G.B., 2015. In vivo histology of the myelin g-ratio with magnetic resonance imaging. Neuroimage 118, 397-405.

Turati, L., Moscatelli, M., Mastropietro, A., Dowell, N.G., Zucca, I., Erbetta, A., Cordiglieri, C., Brenna, G., Bianchi, B., Mantegazza, R., Cercignani, M., Baggi, F., Minati, L., 2015. In vivo quantitative magnetization transfer imaging correlates with histology during de- and remyelination in cuprizone-treated mice. NMR Biomed 28: 327–337.

van den Heuvel, M.P., Sporns, O., 2011. Rich-club organization of the human connectome. J Neurosci 31, 15775-15786.

van den Heuvel, M.P., Sporns, O., 2013. Network hubs in the human brain. Trends Cogn Sci 17, 683-696.

van den Heuvel, M.P., Sporns, O., Collin, G., Scheewe, T., Mandl, R.C., Cahn, W., Goni, J., Hulshoff Pol, H.E., Kahn, R.S., 2013. Abnormal rich club organization and functional brain dynamics in schizophrenia. JAMA Psychiatry 70, 783-792.

van den Heuvel, M.P., Yeo, B.T., 2017. A Spotlight on Bridging Microscale and Macroscale Human Brain Architecture. Neuron 93, 1248-1251.

Vavasour, I.M., Laule, C., Li, D.K., Traboulsee, A.L., MacKay, A.L., 2011. Is the magnetization transfer ratio a marker for myelin in multiple sclerosis? J Magn Reson Imaging. 33: 713–8.

Venkatesan, R., Lin, W., Haacke, E.M., 1998. Accurate determination of spin-density and T1 in the presence of RF-field inhomogeneities and flip-angle miscalibration. Magn Reson Med 40, 592-602.

Wang, R., Benner, T., Sorensen, A.G., Wedeen, V.J., 2007. Diffusion toolkit: a software package for diffusion imaging data processing and tractography. ISMRM Annual Meeting, Berlin.

Wang, S., Young, K.M., 2014. White matter plasticity in adulthood. Neuroscience 276, 148-160.

West, K.L., Kelm, N.D., Carson, R.P., Does, M.D., 2016. A revised model for estimating g-ratio from MRI. Neuroimage 125, 1155-1158.

Whitley, E., Ball, J., 2002, Statistics review 6: Nonparametric methods. Critical Care 6(6): 509-513.

Yang, S., Li, C., Qiu, X., Zhang, L., Lu, W., Chen, L., Zhao, Y.Y., Shi, X.Y., Huang, C.X., Cheng, G.H., Tang, Y., 2013. Effects of an enriched environment on myelin sheaths in the white matter of rats during normal aging: A stereological study. Neuroscience 234, 13-21.

Zhang, H., Schneider, T., Wheeler-Kingshott, C.A., Alexander, D.C., 2012. NODDI: practical in vivo neurite orientation dispersion and density imaging of the human brain. Neuroimage 61, 1000-1016.

ACCEPTED MANUSCRIPT

Figure legends

Figure 1 Schematic overview of the pre-processing pipeline for obtaining NOS- and g-ratio-weighted connectivity matrices from the data. Structural data were processed and parcellated using FreeSurfer, while diffusion data were used to deterministically reconstruct white matter streamlines. NODDI and qMT parametric maps were reconstructed as detailed in the methods in order to compute the g-ratio voxel-wise. Appropriate co-registration was applied to represent both the streamlines and the g-ratio maps in the anatomical space, in order to count the number of streamlines between each pair of regions (NOS-weighted) or evaluating the average g-ratio of each streamline (g-ratio-weighted). In this way, NOS-weighted and G-ratio weighted networks were obtained.

Figure 2 NOS-weighted (left) and g-ratio-weighted (centre) networks with the related g-ratio histograms (right) for the two datasets (top row: dataset A; bottom row: dataset B) averaged across subjects. The networks were averaged taking into considerations only the connections showed by at least the 50% of the subjects in each dataset and computing the average without the null elements as described from de Reus and van den Heuvel (de Reus and van den Heuvel, 2013). The histograms show the g-ratio distribution across the streamlines.

Figure 3 NOS-weighted strength distribution (in blue) and related average g-ratio distribution (in red) for the two datasets. The average g-ratio distribution was sorted first according to the NOS-weighted strength distribution (red dots) and then in ascending g-ratio order (red bars) including the related standard deviation. More details about those distributions are available in the supplementary materials.

Figure 4 Distribution of the g-ratio across connections classes with the related standard deviation (rich-club: top-left; subcortico-cortical: bottom-left; inter-intrahemispheric: bottom-right) and using the s-core decomposition using the NOS-weighted strength (top-right). A star mark was used for indicating specific significant comparisons while two star marks were used for highlighting where all the comparisons were significant ($p<0.05$, Bonferroni corrected).

ACCEPTED MANUSCRIPT

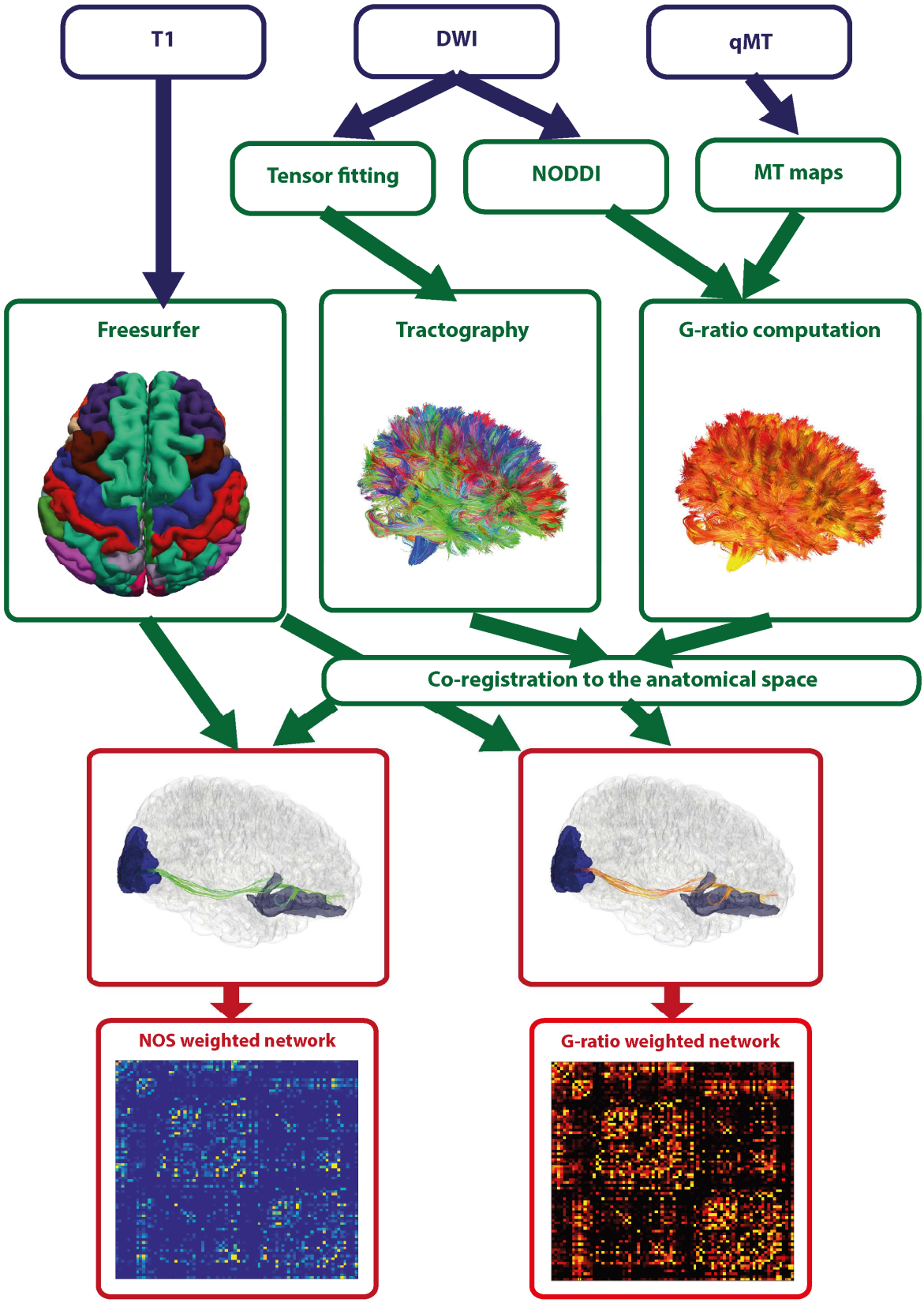
T1
DWI
qMT
Tensor fitting
NODDI
MT maps
Freesurfer
Tractography
G-ratio computation
Co-registration to the anatomical space
NOS weighted network
G-ratio weighted network

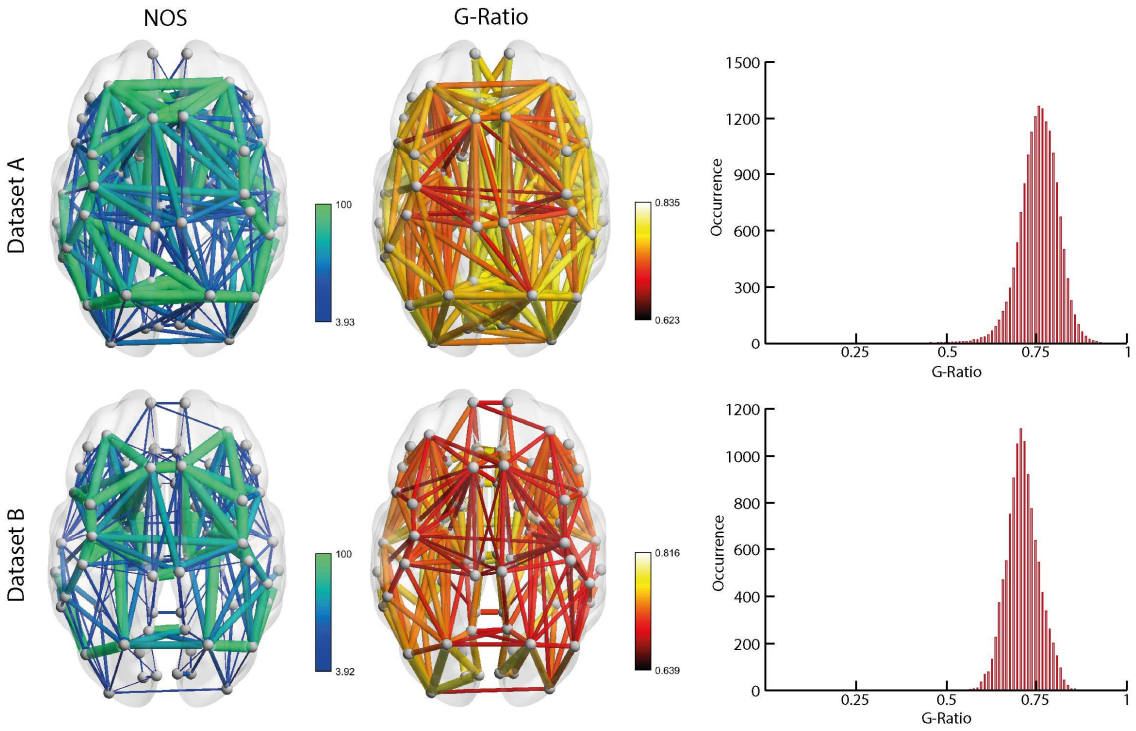
NOS
G-Ratio
Dataset A
Dataset B
100
3.93
0.835
0.623
100
3.92
0.816
0.639
Occurrence
G-Ratio
1500
1200
900
600
300
0
0.25
0.5
0.75
1
1200
1000
800
600
400
200
0

ACCEPTED MANUSCRIPT

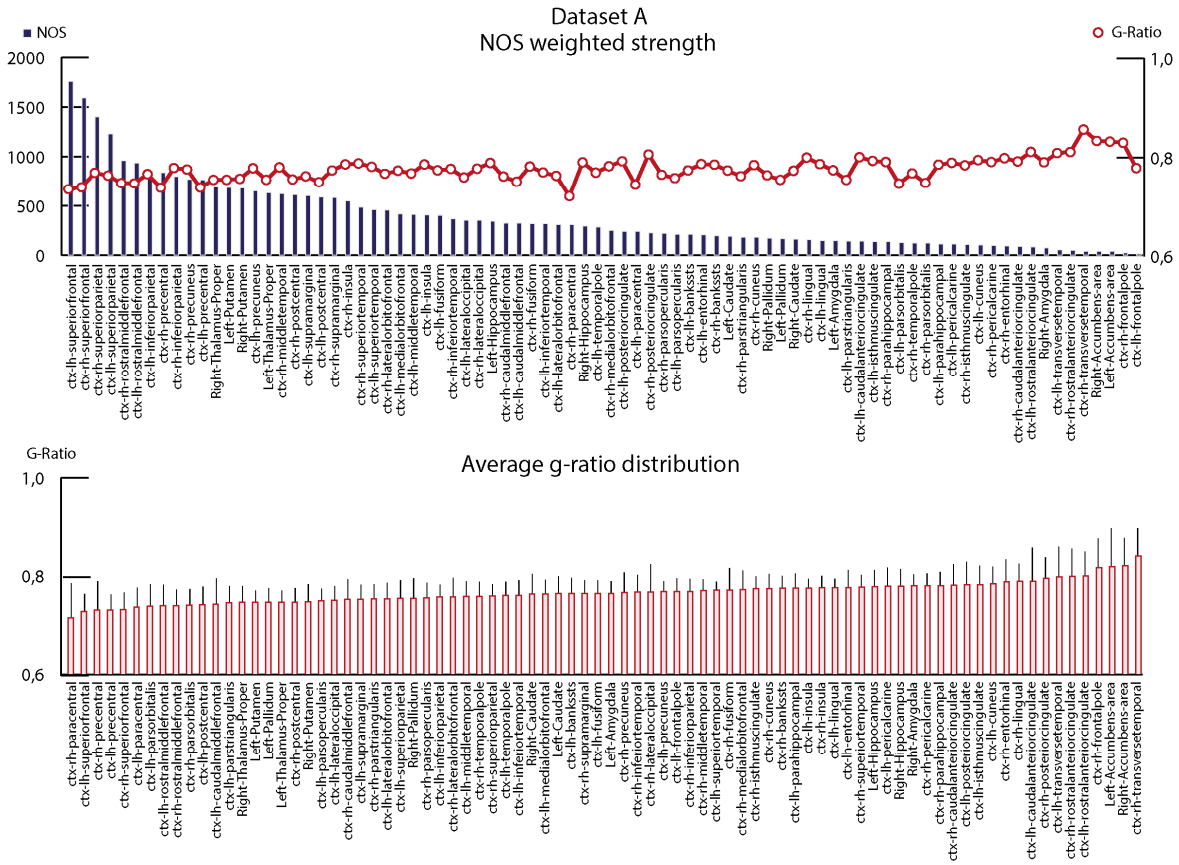

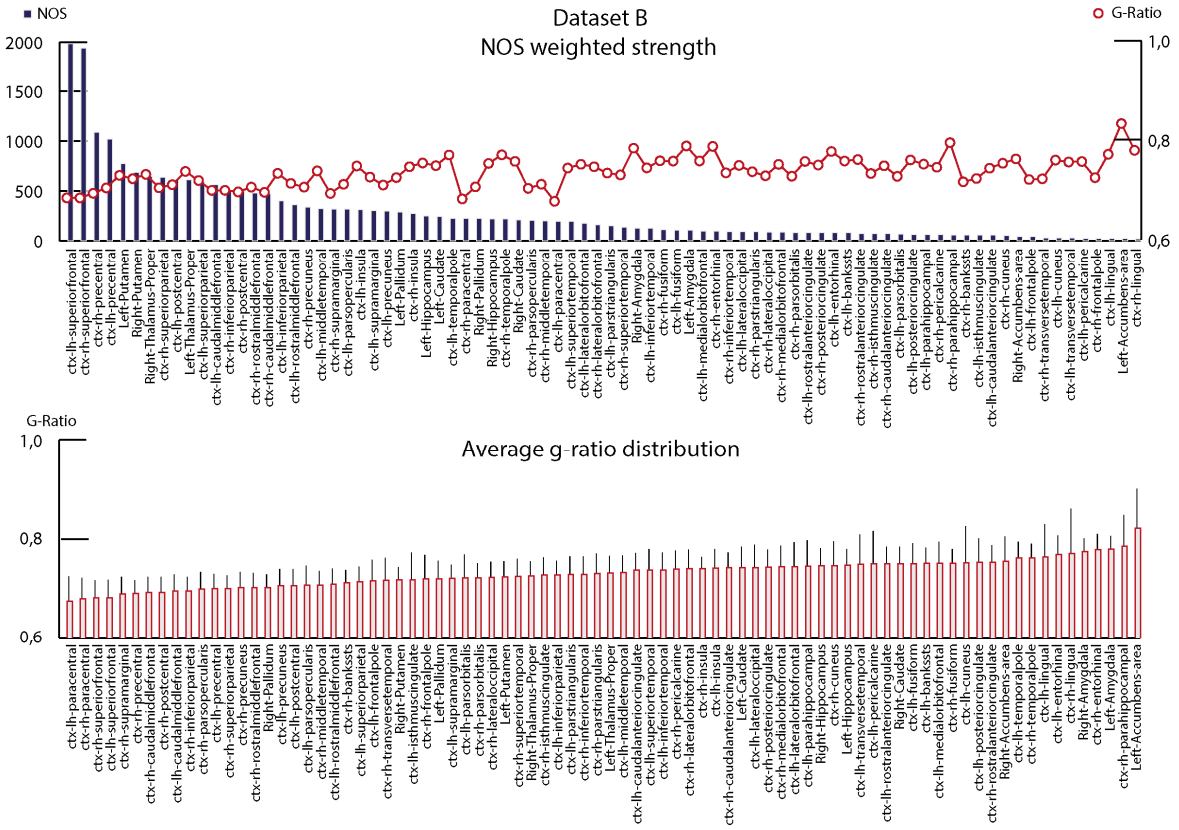

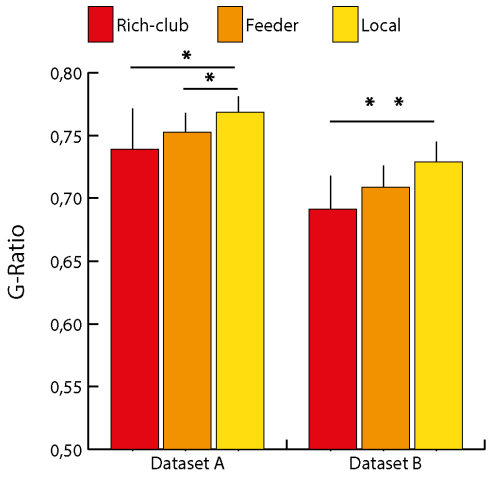
Rich-club
Feeder
Local
G-Ratio
0,80
0,75
0,70
0,65
0,60
0,55
0,50
Dataset A
Dataset B
*
*
* *

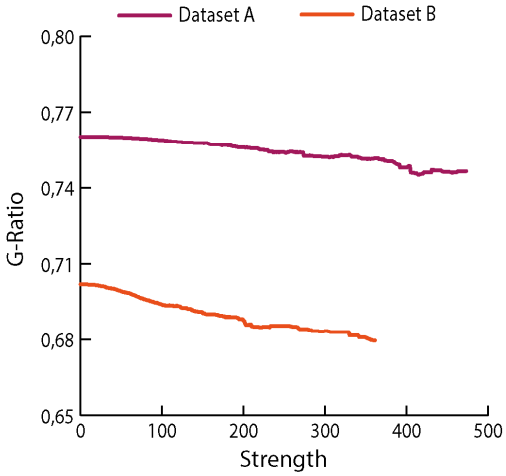
Dataset A
Dataset B
G-Ratio
0,80
0,77
0,74
0,71
0,68
0,65
0
100
200
300
400
500
Strength

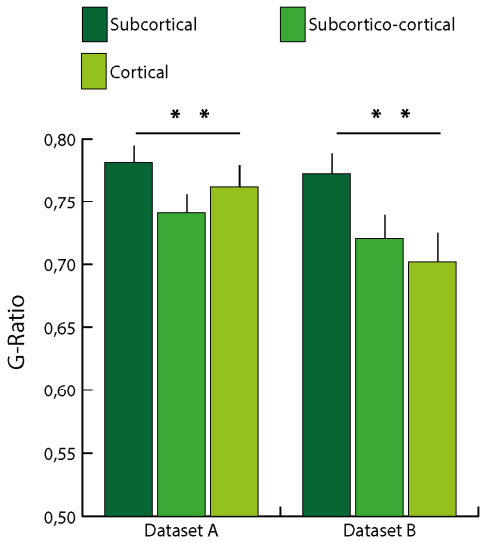
Subcortical
Subcortico-cortical
Cortical
G-Ratio
0,80
0,75
0,70
0,65
0,60
0,55
0,50
Dataset A
Dataset B
* *
* *

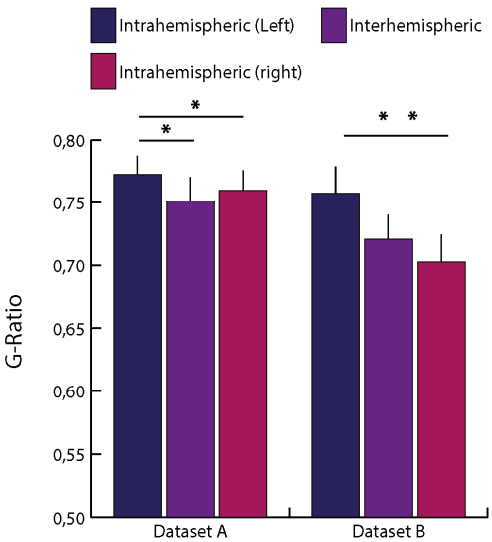
Intrahemispheric (Left)
Interhemispheric
Intrahemispheric (right)
G-Ratio
0,80
0,75
0,70
0,65
0,60
0,55
0,50
Dataset A
Dataset B
*
*
* *